

Article

Fe Doping Enhances the Peroxidase-Like Activity of CuO for Ascorbic Acid Sensing

Boyuan Yan [†], Ying Yang [†], Yinyun Xie [†], Jinzhao Li and Kun Li ^{*†} 

State Key Laboratory of Chemo/Biosensing and Chemometrics, College of Chemistry and Chemical Engineering, Hunan University, Changsha 410082, China

* Correspondence: kunli@hnu.edu.cn

† These authors contributed equally to this work.

Abstract: Although significant advances have been witnessed in the application of nanozymes in recent years, exploring new strategies to enhance the enzyme-like activity of nanozymes is of urgent importance. Herein, we investigate the feasibility of accelerating the peroxidase-like reaction rate of CuO nanostructures through Fe doping. The coprecipitation method was used to synthesize Fe-doped CuO (Fe-CuO) nanozymes, and the results indicate that the diversified valence of Fe benefits the redox reaction driven by CuO-based nanozymes. With the improved peroxidase-like activity, the Fe-CuO nanozyme enables the significant chromogenic oxidation reaction of 3,3',5,5'-tetramethylbenzidine (TMB), facilitating the construction of a visual sensing platform for the sensitive and selective determination of ascorbic acid. Under optimal conditions, the absorbance at 652 nm decreases linearly with the concentration of ascorbic acid in the range of 5–50 μM , with a limit of detection as low as 4.66 μM . This work exemplifies the activity enhancement for peroxidase-mimicking nanozymes with a metal-doping strategy and provides a broad prospect for the design of more high-performance nanozymes for biosensing applications.

Keywords: CuO; nanozyme; peroxidase-like activity; ascorbic acid; colorimetric sensing



Citation: Yan, B.; Yang, Y.; Xie, Y.; Li, J.; Li, K. Fe Doping Enhances the Peroxidase-Like Activity of CuO for Ascorbic Acid Sensing. *Chemistry* **2023**, *5*, 1302–1316. <https://doi.org/10.3390/chemistry5020088>

Academic Editor: Di Li

Received: 5 May 2023

Revised: 19 May 2023

Accepted: 21 May 2023

Published: 23 May 2023



Copyright: © 2023 by the authors. Licensee MDPI, Basel, Switzerland. This article is an open access article distributed under the terms and conditions of the Creative Commons Attribution (CC BY) license (<https://creativecommons.org/licenses/by/4.0/>).

1. Introduction

The biosensing of biomarkers and small molecules is of great significance in biomedicines, the environment, and the food industry [1–3]. A variety of nanomaterials with unique optical, electrical, and catalytic properties and recognition functions play important roles [4–8]. Among them, nanozymes, as a collection of nanomaterials with natural enzyme-like activities, have been used in the field of biosensors to replace natural enzymes because of their high stability, low cost, and ease of mass production [9–15]. Although massive kinds of nanozymes have received tremendous attention over the past years, the catalytic activity of some nanozymes is still relatively low, which restricts their potential applications [16,17]. Notably, as an essential metal element to life, Cu is an important part of many natural enzymes [15]. However, the catalytic activity of various existing Cu-based nanozymes, for example CuO nanozyme, is still lower than that of natural PODs, making the development of new methods to enhance the activity of the CuO nanozyme still challenging.

Recently, various strategies have been developed to enhance the activity of nanozymes [18–20]. For example, higher peroxidase (POD)-like activity can be obtained by fabricating hybrid nanomaterials, tuning the morphology of nanomaterials, or modifying with functional molecules on the surface of nanozymes [14,15]. Another effective route was reported in which doping with suitable heteroatoms could enhance the enzyme-like catalytic activity of nanomaterials. For instance, Mo-doped Co_3O_4 nanotubes endow an enhanced POD-like activity compared with pristine Co_3O_4 nanotubes, which was

Attributed to the additional reaction of oxygen species by the doping elements [21]. Therefore, it was a great opportunity to improve the POD-like activity by preparing novel types of heteroatom-doped CuO nanomaterials.

Fe₃O₄ is considered to be the first reported metal-based nanozymes [9]. The diversified valence of Fe benefits the redox reaction driven by the nanozyme which acts similarly to the natural oxidoreductase. Thus, we are inspired to introduce Fe into CuO nanostructures to improve the POD-like activity of CuO nanozyme. In this contribution, Fe-doped CuO (Fe-CuO) nanostructures are first fabricated using a coprecipitation method. After verifying that the Fe-CuO nanozyme only possesses POD-like activity, the steady-state kinetics are systematically investigated and the roles of radicals in the Fe-doping-enhanced nanozymatic catalysis are studied. Moreover, we figure out the linear relationship between the concentration of H₂O₂ and the absorbance of the colorimetric reaction. Thus, a fast colorimetric sensing strategy based on the Fe-CuO nanozyme is proposed for the highly sensitive and selective detection of ascorbic acid (AA). Additionally, on the basis of the superior POD-like activity of the Fe-CuO nanozyme, we constructed a total antioxidant capacity (TAC) biosensor with AA as an antioxidant model by expressing TAC as an AA-equivalent antioxidant capacity.

2. Materials and Methods

2.1. Chemicals

FeCl₂·4H₂O, CuCl₂·2H₂O, NaOH, hydrogen peroxide (H₂O₂, 30% wt), ascorbic acid (AA), glycine (gly), lysine (lys), phenylalanine (phe), glucose, KCl, and CaCl₂ were purchased from the Sinopharm Chemical Reagents Co., Ltd. 3,3',5,5'-tetramethylbenzidine (TMB), terephthalic acid (TA), and 5,5-dimethyl-1-pyrroline 1-oxide (DMPO) were purchased from Adamas beta. All chemicals are of analytical grade without further purification before use. Ultrapure water (18.25 MΩ·cm⁻², 25 °C) used in the experiment is from the Millipore Milli-Q system.

2.2. Apparatus and Characterization

The morphologies of CuO and Fe-CuO were characterized using a JEM-2100 Plus (JEOL, Tokyo, Japan) transmission electron microscope (TEM) operating at 300 kV. X-ray diffraction (XRD) patterns were carried out on a D8 (Bruker, Karlsruhe, Germany) using Ni-filtered Cu Kα radiation ($l = 1.5406 \text{ \AA}$). The UV-Vis spectra were recorded at room temperature on a UV-2600 (Shimadzu, Kyoto, Japan) using a quartz cuvette with an optical path of 10 mm. Fluorometric data were obtained on a spectrofluorophotometer (F-7000, Hitachi, Tokyo, Japan).

2.3. Preparation of CuO and Fe-CuO

The preparation of CuO and Fe-CuO was carried out using a coprecipitation method as described in previous work with little modification [22]. The doped and undoped CuO nanostructures were prepared in a 50 mL flask. First, 248.5 mg of FeCl₂·4H₂O and 1917.9 mg of CuCl₂·2H₂O were dissolved in 25.0 mL water and stirred for 30 min at room temperature. After the addition of 5.0 mL of NaOH (15.0 M), the solution was stirred for 2 h at 70 °C. Subsequently, the colloidal solution was cooled down to room temperature. The resulting product was centrifuged at 5000 rpm for 10 min and washed with ultrapure water and acetone twice each to remove the unused salts. The precipitate was dried under a vacuum oven at 373 K for 2 h and ground in a mortar to make fine powders.

2.4. POD-like Activity Assay for Fe-CuO Nanozymes

The peroxidase activity of undoped CuO and Fe-CuO nanozymes was studied using the catalytic oxidation of TMB with H₂O₂. In a typical experiment, 36 μL of TMB solution (10 mg·mL⁻¹) and 150 μL of H₂O₂ (100 mM) were added to acetate buffer (pH 4.0) at 25 °C. Then, 270 μL of CuO or Fe-CuO nanozymes (1 mg·mL⁻¹) were introduced to make the final acetate (0.2 M) buffered solution of 3 mL. After 5 min of reaction, the solution was filtered using an ultrafilter film to collect the filtrate. The UV-Vis spectrum and the absorbance at 652 nm of the filtrate were measured using a UV-Vis spectrophotometer.

To calculate kinetic parameters, the Michaelis–Menten equation and its Lineweaver–Burk double reciprocal representation were used:

$$V = \frac{V_{max} [S]}{K_m + [S]}$$

$$\frac{1}{V} = \frac{K_m}{V_{max}} \cdot \frac{1}{[S]} + \frac{1}{V_{max}}$$

where V_0 and V_{max} are the initial and maximum reaction velocities, respectively. $[S]$ represents the substrate concentration. K_m represents the Michaelis–Menten constant.

To determine the POD-like catalytic kinetic parameters, 90 $\mu\text{g}\cdot\text{mL}^{-1}$ of CuO and Fe-CuO were used in 0.2 M acetate buffer (pH 4.0) to measure the initial reaction rate at 25 °C. When evaluating the kinetic parameters obtained for TMB or H_2O_2 as the substrate, a constant concentration of H_2O_2 (5 mM) or TMB (0.12 $\text{mg}\cdot\text{mL}^{-1}$) was used, respectively. The V_0 value is calculated using the following equations:

$$V_0 = \frac{c}{t}$$

$$c = \frac{A}{b \times \epsilon_{652}}$$

where A and t represent the absorbance of oxTMB at 652 nm and the reaction time, respectively. $\epsilon_{652} = 39,000 \text{ M}^{-1}\cdot\text{cm}^{-1}$ and $b = 1 \text{ cm}$.

2.5. Detection of AA Using Fe-CuO Nanozymes

Colorimetric detection of AA was carried out as follows. First, 36 μL of TMB solution (10 $\text{mg}\cdot\text{mL}^{-1}$), 45 μL of H_2O_2 (10 mM), and a series of AA solutions with various concentrations were added to acetate buffer (pH 4.0) at 25 °C. Then, 270 μL of Fe-CuO nanozyme (1 $\text{mg}\cdot\text{mL}^{-1}$) was introduced to make the final acetate (0.2 M) buffered solution of 3 mL. After 5 min of reaction, the solution was filtered using an ultrafilter film to collect the filtrate. The absorbance at 652 nm of the filtrate was measured using a UV-Vis spectrophotometer. The experiment was repeated three times under the same conditions. The limit of detection (LOD) was calculated as $\text{LOD} = 3\sigma/k$, where σ is the standard deviation of the experiment and k is the slope of the linear curve.

2.6. TAC Assay

A commercial beverage (Mizone) was used for the TAC assay. The above-mentioned protocol for AA detection was employed. The beverage was diluted appropriately for the sample preparation. After the addition of 30 μL sample, the reaction of 3 mL system containing 120 $\mu\text{g}\cdot\text{mL}^{-1}$ TMB, 150 μM H_2O_2 , and 90 $\mu\text{g}\cdot\text{mL}^{-1}$ Fe-CuO nanozyme in 0.2 M acetate buffer (pH 4.0) was conducted at 25 °C for 5 min. In the spiked recovery experiments, the standard AA solution with the concentration of 1 mM was introduced to calculate the recovery.

3. Results and Discussion

3.1. Characterization of CuO and Fe-CuO Nanozymes

To prepared CuO-based POD-mimicking nanozymes, CuO and Fe-doped CuO (Fe-CuO) nanostructures were synthesized using a classical coprecipitation method (Figure 1). The expected molar ratio of Fe and Cu is 1:9 for Fe-CuO. Thus, for the preparation of doped nanostructures with a nominal composition of $\text{Fe}_x\text{Cu}_{1-x}\text{O}$ ($x = 0.1$), FeCl_2 is mixed with CuCl_2 in the stoichiometric ratio first. The addition of NaOH at 70 °C induces the reactions as follows.

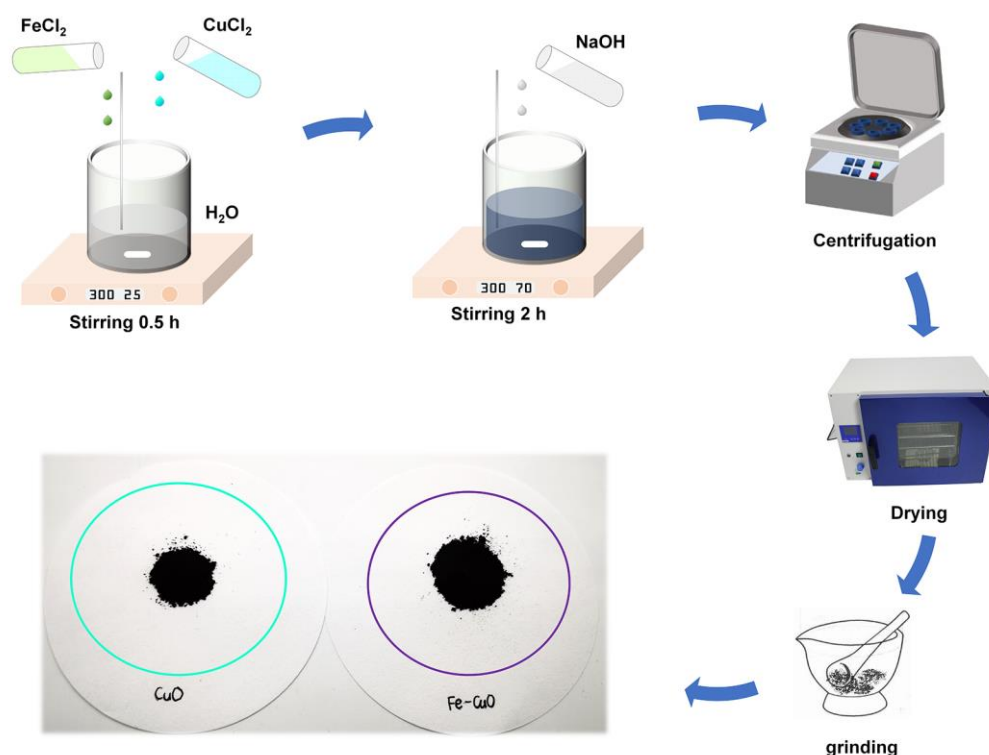
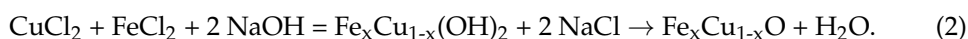


Figure 1. Scheme for the preparation of CuO and Fe-CuO nanozymes and the digital photograph of the synthesized CuO and Fe-CuO nanozymes.

For undoped CuO,



For doped Fe-CuO,



After the resultant solution was filtered, washed, and dried, it was seen that the prepared samples were fine powders with dark colors (Figure 1).

The morphologies of CuO and Fe-CuO were characterized using SEM. Figure 2a,b indicates that CuO nanostructures have leaf-like profiles, while Fe-CuO nanostructures look more like rough leaves with major veins and rods. The change in morphology should be ascribed to the interstitial of Fe ions at Cu sites in the CuO lattice. Moreover, we conducted an elemental analysis of CuO and Fe-CuO to prove the successful introduction and uniform distribution of Fe (Figure 2c,d). The EDX spectrum further confirms that only copper and oxygen elements appear in CuO (Figure 2e). On the contrary, Fe-CuO nanostructures have an Fe/Cu weight ratio of 1:13.3 and an Fe/Cu atomic ratio of 1:11.6 (Figure 2f), which confirm that the elemental stoichiometry is basically in accordance with the ratio of the precursors used in the synthetic procedure.

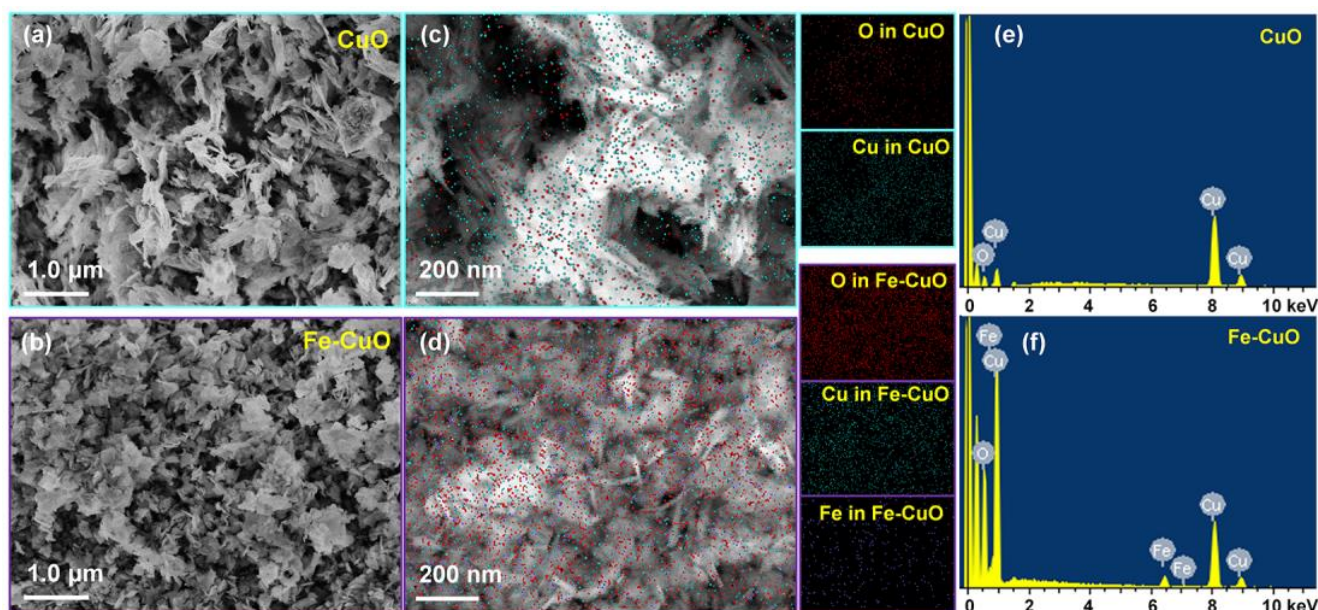


Figure 2. SEM images of the synthesized CuO (a) and Fe-CuO (b) nanozymes. Elemental analysis images of the synthesized CuO (c) and Fe-CuO (d) nanozymes. In panel (c) and (d), the red, cyan, and purple dots indicates the appearance of O, Cu, and Fe, respectively. EDX spectra of the synthesized CuO (e) and Fe-CuO (f) nanozymes.

Representative TEM images further reveal the flat nanostructures of CuO and the rough nanostructures of Fe-CuO (Figure 3a,b). These patterns are well corroborated with the surface morphology results obtained from SEM. In addition, we examined the XRD patterns of CuO and Fe-CuO for the crystal structure and phase analysis (Figure 3c). The diffraction peaks could be indexed to the phase of CuO (JCPDS#48-1548). Interestingly, it is noted that characteristic peaks remain unchanged after doping with Fe. This indicates that the crystal structure of CuO is not distorted in Fe-CuO, which may result from the similarity of the ionic radii of Fe and Cu. Therefore, the above investigations verify the successful preparation of Fe-CuO with the uniform doping of Fe.

3.2. Fe-Doping-Enhanced Peroxidase-like Activity of CuO

Five different reaction systems were designed to study the influence of Fe doping on the peroxidase-like catalytic property of CuO (Figure 4a). TMB is a commonly used substrate for the chromogenic oxidation reaction catalyzed by peroxidases with the presence of H_2O_2 . During the reaction, the amino group of TMB loses an electron to become a cationic free radical and forms a charge-transfer complex which has maximum absorptions at 371 nm and 652 nm, gifting the oxTMB a characteristic blue color [23]. The oxidation of TMB by H_2O_2 under different conditions is displayed in Figure 4b. Compared with the reaction catalyzed by the CuO nanozyme (curve #2), the doping of Fe results in a significant increase in the absorption at 652 nm for the Fe-CuO nanozyme (curve #1). As a comparison, the Fe-CuO nanozyme cannot catalyze the reaction between O_2 and TMB (curve #3), indicating that the Fe-CuO nanozyme does not possess an obvious oxidase-like activity. Moreover, it is not surprising to find that neither the reaction between H_2O_2 and TMB without any catalysts (curve #4) nor the reaction system in the absence of TMB as a visible indicator (curve #5) exhibit a negligible absorbance. The above results substantiate that Fe doping enhances the POD-like activity of CuO in the proposed Fe-CuO nanozyme.

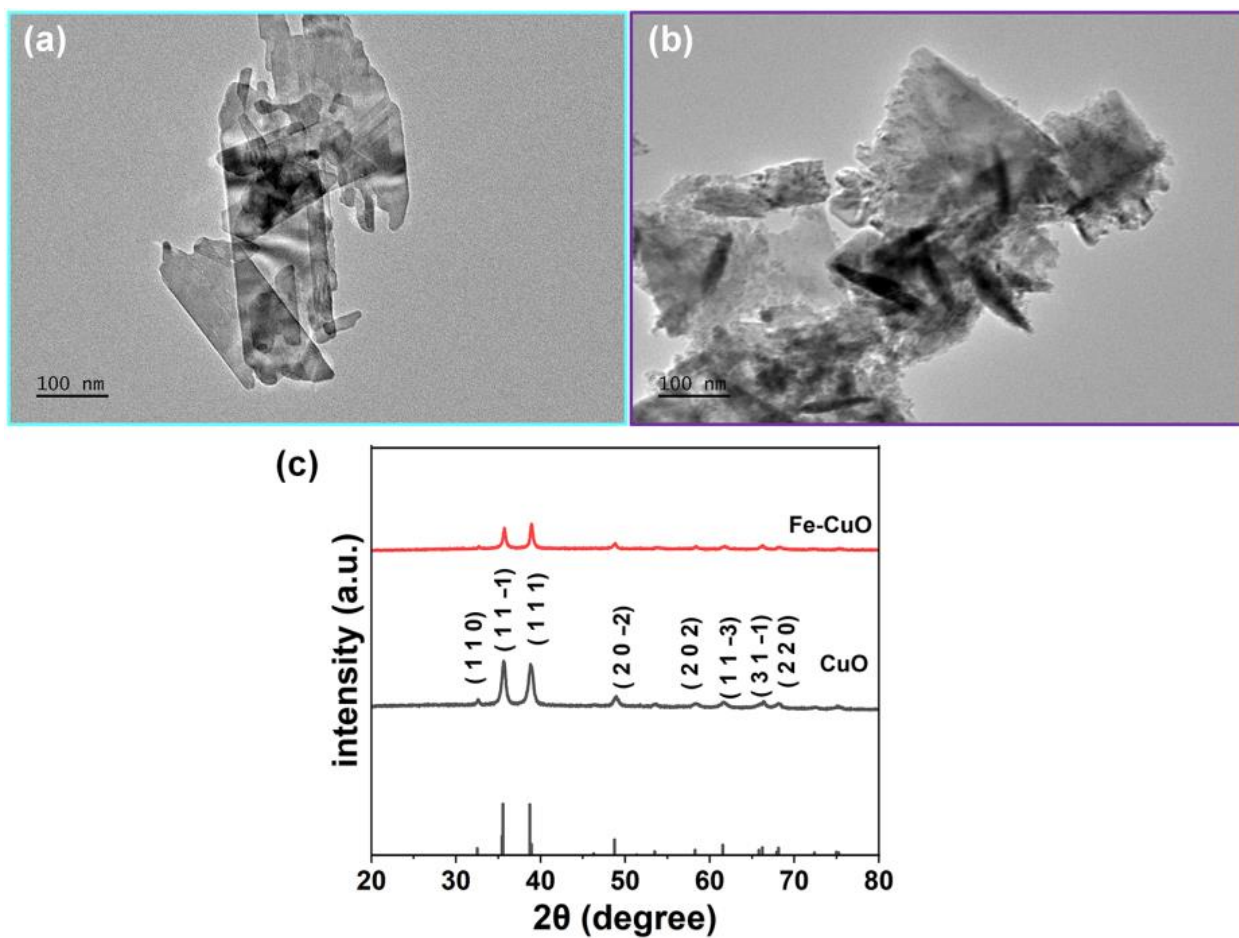


Figure 3. TEM images of the synthesized CuO (a) and Fe-CuO (b) nanozymes. (c) XRD results of the synthesized CuO and Fe-CuO nanozymes.

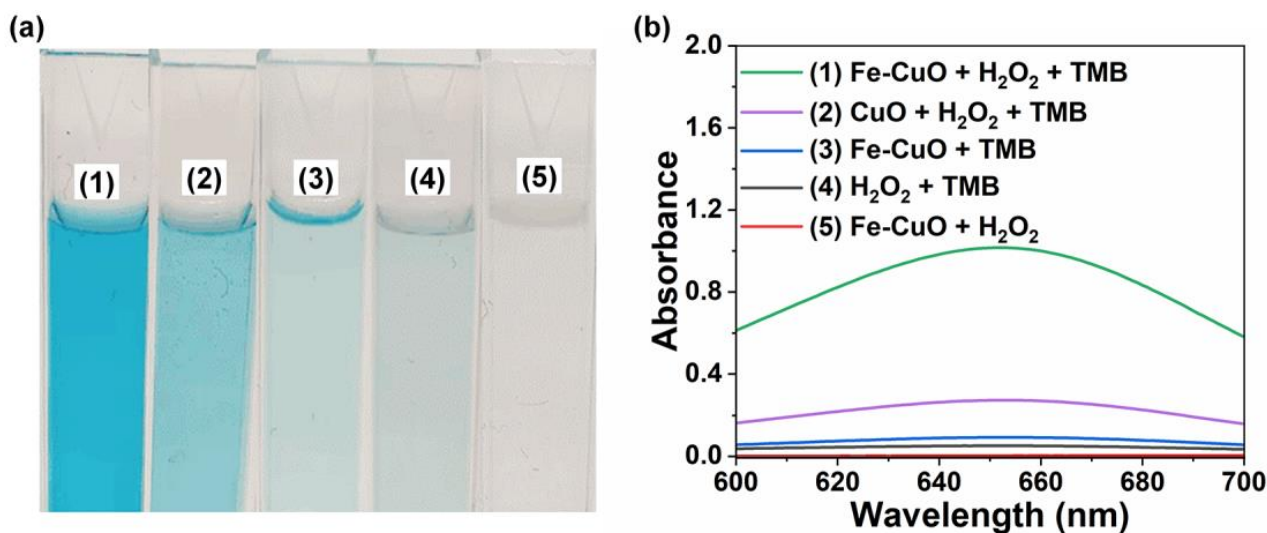


Figure 4. (a) Photographs of different reaction systems. (b) The corresponding UV-Vis absorption spectra of different reaction systems. Systems (1–5) shown in panel (a) are identical to those in panel (b). The reactions of 3 mL system containing $120 \mu\text{g}\cdot\text{mL}^{-1}$ TMB, 5 mM H₂O₂, and 90 $\mu\text{g}/\text{mL}$ CuO or Fe-CuO nanozyme in 0.2 M acetate buffer (pH 4.0) were conducted at 25 °C for 10 min.

3.3. Steady-State Kinetic Assay

As is known, the catalytic behaviors of enzyme mimics follow the Michaelis–Menten equation. To further understand the peroxidase-like catalytic activity of CuO enhanced by Fe doping, the kinetic parameters of CuO and Fe-CuO nanozymes were analyzed and compared. By fixing the concentration of one substrate (TMB or H₂O₂) and varying the concentration of the other substrate, the initial catalytic rates for both CuO and Fe-CuO were tested. Thus, we obtained the reaction velocity vs. substrate concentration curves, which follow the classic Michaelis–Menten equation (Figure 5, insets). Furthermore, the catalytic kinetic parameters (V_{\max} and K_m) of H₂O₂ and TMB were calculated by using the double reciprocal Lineweaver–Burk diagram (Figure 5).

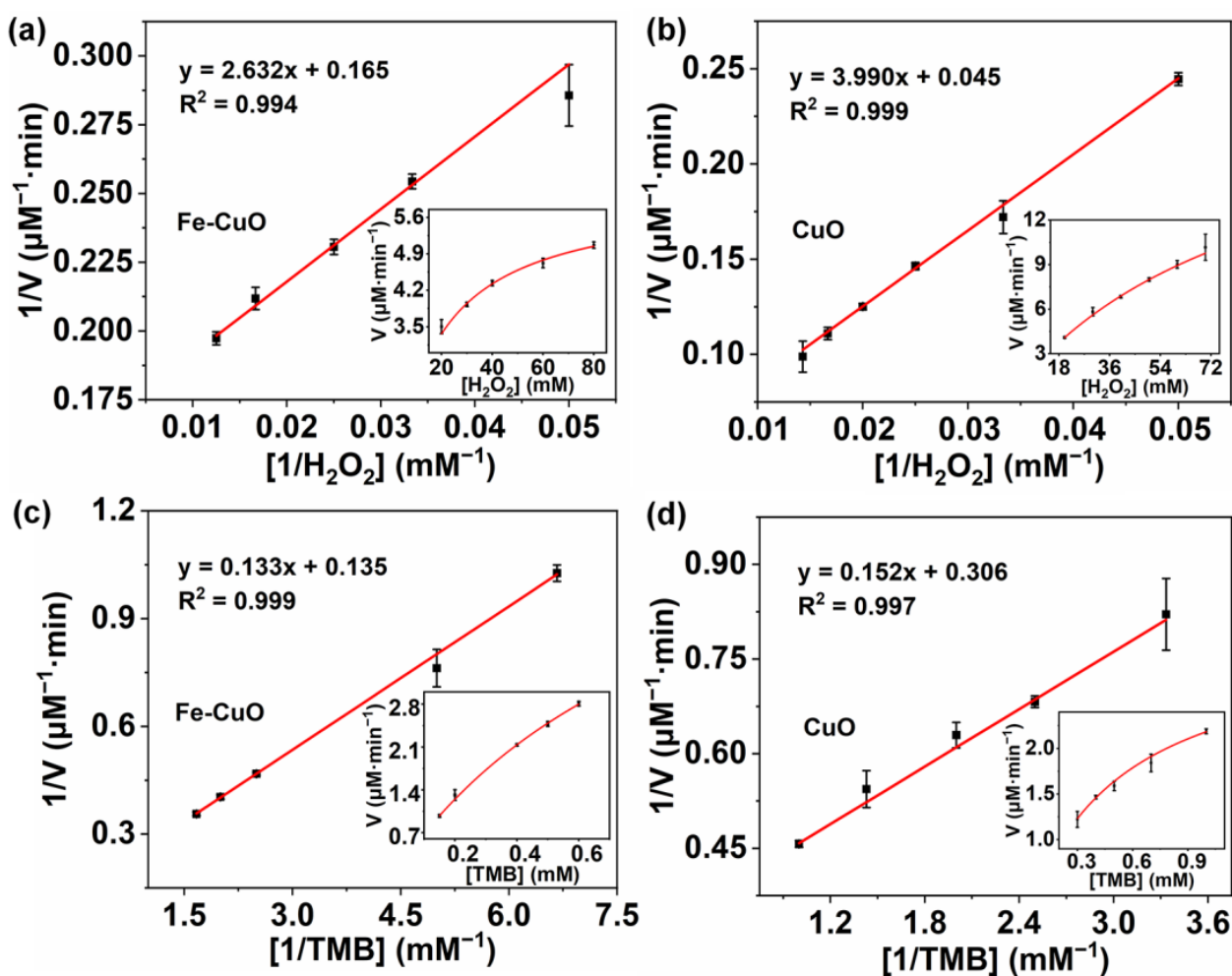


Figure 5. (a) Lineweaver–Burk plot (inset: Michaelis–Menten kinetics) of the nanozymatic activity of Fe-CuO with H₂O₂ as the substrate. (b) Lineweaver–Burk plot (inset: Michaelis–Menten kinetics) of the nanozymatic activity of CuO with H₂O₂ as the substrate. (c) Lineweaver–Burk plot (inset: Michaelis–Menten kinetics) of the nanozymatic activity of Fe-CuO with TMB as the substrate. (d) Lineweaver–Burk plot (inset: Michaelis–Menten kinetics) of the nanozymatic activity of CuO with TMB as the substrate. The reactions of a 3 mL system containing 120 $\mu\text{g}\cdot\text{mL}^{-1}$ TMB, 5 mM H₂O₂, and 90 $\mu\text{g}/\text{mL}$ CuO or Fe-CuO nanozyme in 0.2 M acetate buffer (pH 4.0) were conducted at 25 °C for 2 min to obtain the initial velocity of the reaction. Error bars in all graphics represent the standard deviation from three repetitive experiments.

In enzymatic catalysis, the value of K_m indicates the affinity of the enzyme and substrates. For both CuO and Fe-CuO nanozymes, the K_m and V_{max} for H_2O_2 and TMB are summarized in Table 1. It is seen that, when using H_2O_2 as the substrate, the K_m of Fe-CuO is 15.9 mM, which is 5.5 times lower than that of CuO ($K_m = 87.9$ mM). The results suggest that Fe-CuO possesses a stronger affinity to H_2O_2 in comparison with CuO. Interestingly, we find that the affinity to TMB of Fe-CuO ($K_m = 0.986$ mM) is slightly lower than that of CuO ($K_m = 0.497$ mM). It is rationally speculated that a typical ping-pong mechanism occurs over the Fe-CuO nanozyme, which indicates that the Fe-CuO nanozyme reacts with the first substrate and then releases the first product before reacting with the second substrate. However, the V_{max} of Fe-CuO for TMB is larger than that of CuO for TMB. The faster reaction rates for the colorimetric substrate make up for the deficiency of weak affinity between Fe-CuO and TMB to a certain extent, suggesting an accelerated rate of enzymatic conversion of the substrate by the CuO-based nanozyme after Fe is doped. Since Fe doping strengthens the POD-like activity of CuO, the kinetic parameters (including K_m and V_{max}) of the Fe-CuO nanozyme are comparable to other state-of-the-art POD-mimicking nanozymes reported recently (Table 1).

Table 1. Comparison of the kinetic parameters of the Fe-CuO nanozyme, CuO nanozyme, and other catalysts with POD-like activity for catalyzing TMB and H_2O_2 reaction at room temperature.

Catalysts	K_m (mM)		V_{max} ($\mu\text{M}/\text{min}$)		References
	H_2O_2	TMB	H_2O_2	TMB	
Fe-CuO	15.9	0.986	6.05	7.40	This work
CuO	87.9	0.497	22.03	3.27	
HRP	3.7	0.434	5.23	6.0	[9]
Cu(PDA)(DMF)	28.6	0.169	1.9	1.32	[24]
$Fe_3O_4@C$ NWs	0.23	0.20	1.45	0.80	[25]
$Fe_3O_4@C/Ni$ NW	0.059	0.10	2.17	2.34	[26]
Por-CuCo ₂ O ₄	9.96	0.044	4.97	5.96	[27]
Au/Cu ₂ O	10.56	0.21	4.01	3.65	[28]
MoS ₂ -CPBNPs	3.17	0.22	0.89	3.82	[29]
MIL-88B-NH ₂ /Pt	0.026	0.00213	1.24	0.62	[30]
Por-CoMoO ₄	0.63	0.26	1.23	56.81	[31]
Pc(OH) ₈ -CoFe LDH	1.55	0.361	2.86	7.47	[32]

3.4. Reactive Oxygen Species in the Nanozymatic Catalysis

To further confirm the catalytic mechanism of the Fe-CuO nanozyme, we investigated reactive oxygen species as they are usually known to be produced in nanozymatic catalysis. It is known that DMPO is a kind of free radical scavenger, which can specifically combine with short-lived hydroxyl ($\bullet\text{OH}$) radicals to form longer-lived DMPO-OH \bullet . Thus, by simply adding DMPO to the catalytic reaction, $\bullet\text{OH}$ radicals will be trapped to generate the aforementioned long-lived radical adducts. Therefore, it can be qualitatively judged whether $\bullet\text{OH}$ radicals are produced from the ESR measurement. Therefore, we performed ESR spectroscopy analysis for the determination of $\bullet\text{OH}$ radicals. A total of 20 μL of as-prepared Fe-CuO dispersion ($4\text{ mg}\cdot\text{mL}^{-1}$), 20 μL of H_2O_2 (100 mM), and 20 μL of DMPO aqueous solution (1 M) were sequentially added into a final solution of 200 μL containing 200 mM acetate buffer (pH 4.0). The mixture was reacted for 10 min before recording the EPR spectra. Figure 6a clearly shows that the characteristic quartet peak of $\bullet\text{OH}$ radicals (1:2:2:1) exists in the Fe-CuO and H_2O_2 mixture system, which suggests that a Fenton-like reaction occurs in TMB oxidation. In addition, $\bullet\text{OH}$ radicals in the system were also investigated using the oxidation of terephthalic acid (TA), which reacts with $\bullet\text{OH}$ radicals to produce 2-hydroxyterephthalic acid exhibiting a strong emission peak at 450 nm. Figure 6b indicates that the Fe-CuO nanozyme can catalyze H_2O_2 into $\bullet\text{OH}$ radicals (black curve). While the other systems (including the system of Fe-CuO and TA, the system of H_2O_2 and TA, and the system of TA only) do not exhibit notable fluorescence

peaks, respectively. These results further confirm that the TMB oxidation originates from $\bullet\text{OH}$ radicals. Accordingly, we propose that the POD-like activity of the Fe-CuO nanozyme is ascribed to the Fenton-type mechanism.

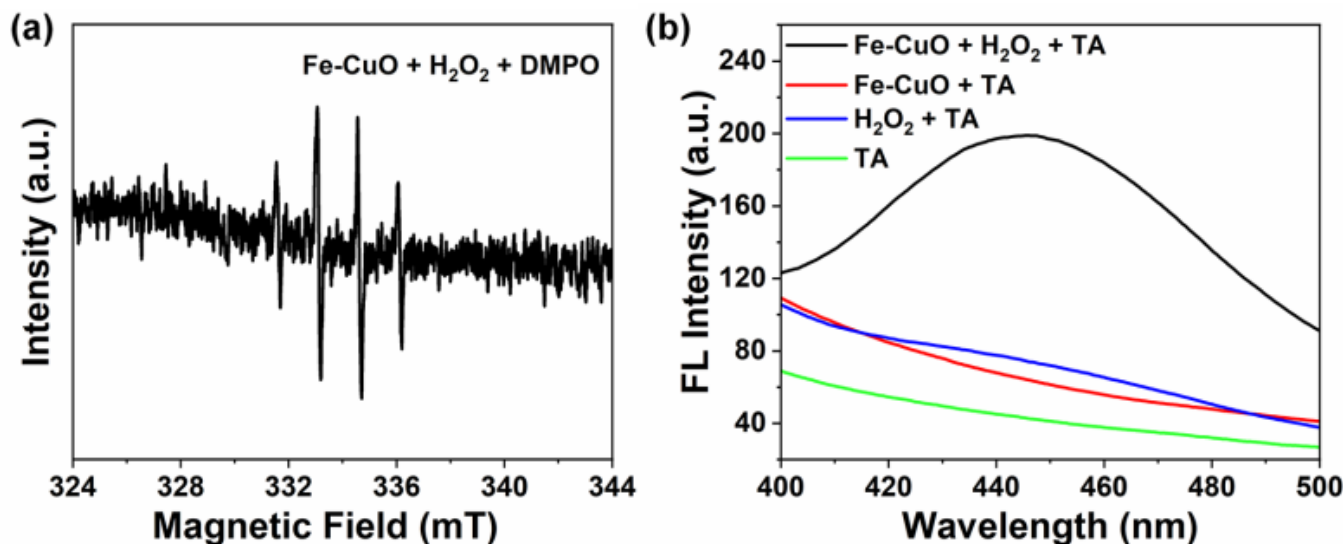


Figure 6. (a) Electron spin resonance (ESR) spectra of $\bullet\text{OH}$ radicals in the reaction system containing 5,5-dimethyl-1-pyrroline N-oxide (DMPO) as the spin trap. The reactions of a 0.2 mL system containing 100 mM DMPO, 10 mM H_2O_2 , and 400 $\mu\text{g}/\text{mL}$ Fe-CuO nanozyme in 0.2 M acetate buffer

(pH 4.0) were conducted at 25 °C for 10 min before the ESR measurement. (b) Fluorescence emission spectra of different reaction systems excited by 315 nm light. The reactions of a 0.5 mL system containing 10 mM TA, 20 mM H_2O_2 , and 320 $\mu\text{g}/\text{mL}$ Fe-CuO nanozyme in 0.2 M acetate buffer (pH 4.0) were conducted at 25 °C for 5 min before fluorescence measurements.

3.5. H_2O_2 Concentration-Dependent Colorimetric Signals Using Fe-CuO Nanozyme

On the basis of the above results, we constructed a platform for H_2O_2 detection by monitoring the absorption intensity changes of oxTMB at 652 nm [33]. To achieve higher sensitivity, the dependence of the reaction system on the concentration of the Fe-CuO nanozyme, pH of the reaction system, reaction temperature, and reaction time were systematically investigated to figure out the optimized experimental conditions of the sensing strategy (Figure 7).

The concentration of the catalyst will greatly affect the intensity of the colorimetric signal, so it needs to be optimized first. By comparing the absorbance of different Fe-CuO nanozyme concentrations, it is found that as the concentration increases from 0 to 210 $\mu\text{g}\cdot\text{mL}^{-1}$; the absorbance of oxTMB at 652 nm gradually increases (Figure 7a). The low catalyst concentration only causes a weak signal; however, too many catalyst nanoparticles affect the light transmittance of the resultant solution and cause a waste of the materials. Therefore, 90 $\mu\text{g}\cdot\text{mL}^{-1}$ of Fe-CuO nanozyme was used as the catalyst concentration for subsequent experiments.

For lots of nanozymes, the pH of the reaction system is a key factor that influences the POD-like activity. Thus, the effect of different pHs (3.0, 3.5, 4.0, 4.5, 5.0, and 5.5) was also investigated (Figure 7b). It is found that the nanozyme system has good POD-like activity in the range of pH from 3.0 to 5.0. As a result, pH 4.0 was selected as the optimal pH for subsequent experiments.

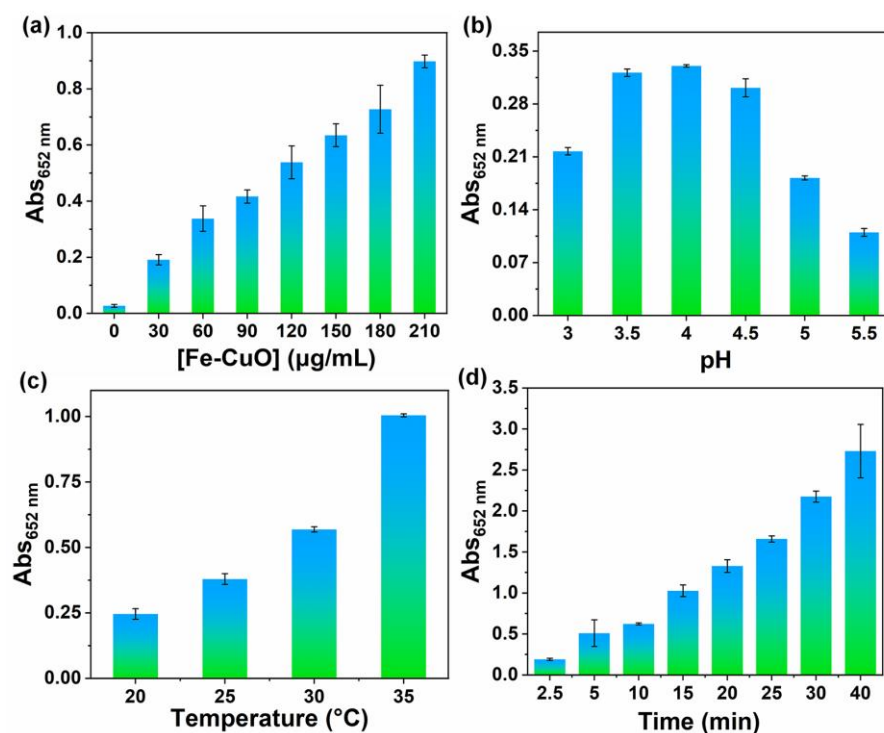


Figure 7. The optimizations of experimental conditions for H₂O₂-induced TMB catalyzed by Fe-CuO nanozyme. The reactions were conducted in 0.2 M acetate buffer containing 100 µg·mL⁻¹ TMB and 5 mM H₂O₂ with various concentrations of Fe-CuO nanozyme (a), pHs of the reaction system (b), temperatures (c), and reaction times (d). Other fixed reaction conditions were 90 µg/mL Fe-CuO nanozyme, pH 4.0, 25 °C, and 5 min. All experiments were repeated three times.

Moreover, in addition to the catalyst concentration and pH of the reaction system, the effect of the reaction temperature is also very important. When the temperature varies from 20 to 35 °C, the absorbance value of oxidized TMB is continuously increased (Figure 7c). Considering the convenience of conducting the nanozymatic reaction procedure, 25 °C was chosen as the optimal temperature for subsequent experiments.

Lastly, the reaction time was explored based on the optimal conditions of 90 µg·mL⁻¹ of Fe-CuO nanozyme, pH 4.0, and 25 °C (Figure 7d). As the incubation time prolongs, the absorbance of oxTMB gradually increases during 45 min. Therefore, in order to save the detecting time for H₂O₂ assay, 5 min was selected as the reaction time for subsequent experiments.

Encouraged by the optimization of experimental conditions, we constructed a colorimetric H₂O₂ bioassay. It is seen that as the H₂O₂ concentration rises, an obvious color change from colorless to blue occurs (Figure 8a). Therefore, we obtained a linear range of 5–150 µM with a limit of detection (LOD) of 7.07 µM (Figure 8b).

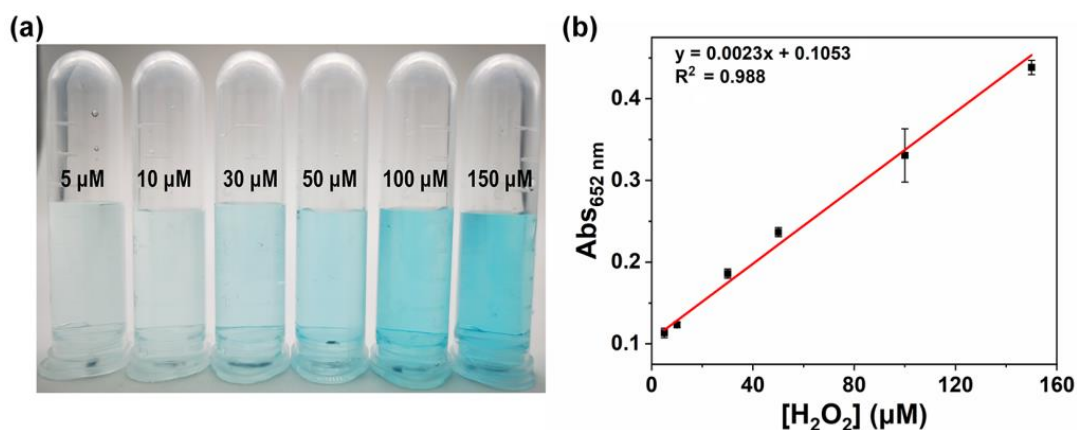


Figure 8. (a) Digital photograph of the resultant systems in the presence of H_2O_2 with different concentrations (5, 10, 30, 50, 100, and 150 μM). (b) Linear calibration plot for H_2O_2 detection from 5 to 150 μM . The reactions of 3 mL system containing $120 \mu\text{g}\cdot\text{mL}^{-1}$ TMB and $90 \mu\text{g}\cdot\text{mL}^{-1}$ Fe-CuO nanozyme in 0.2 M acetate buffer (pH 4.0) were conducted at 25 °C for 5 min. Error bars in panel (b) are the standard deviations of three parallel experiments.

3.6. Analytical Performance of Fe-CuO Nanozyme-Based AA Detection

Ascorbic acid (AA), is one of the important vitamins that can participate in many important biological reactions to adjust the normal physiological function of the body [34]. AA is also considered to be an important indicator of the freshness and nutritional quality of fruits [35]. Thus, it is vital to develop fast and sensitive methods for detecting AA. As a typical reducing agent, AA can effectively reduce oxTMB to its reduction form, leading to a discoloration of the solution. By introducing AA to the chromogenic TMB oxidation reaction catalyzed by Fe-CuO nanozymes, the shade of the blue color can reflect the amount of AA. Accordingly, we are inspired to develop a colorimetric AA sensing strategy by utilizing the improved POD-like activity of Fe-CuO nanozymes (Figure 9a).

Figure 9b shows that the blue color of the resultant solution becomes lighter as the concentration of AA increases. Thus, a good linear relationship between the absorbance at 652 nm and AA concentration is established in the range from 5 to 50 μM with $R^2 = 0.991$ (Figure 9c). The results are averaged values obtained from three repetitive measurements under the same experimental conditions, which represent a good reproducibility of the method. At a signal-to-noise ratio (S/N) of 3, the limit detection for AA is calculated to be 4.66 μM , which is comparable to the AA detection methods proposed in recent reports (Table 2). The results of this analysis indicate that the high sensitivity of AA detection with Fe-CuO nanozymes has a good usability.

Table 2. Comparison of the present work for AA detection with recently reported methods.

Materials	Linear Range	LOD	Reference
Fe-CuO	5–50 μM	4.66 μM	This work
CP (600C–6)	0.8–80 μM	35 μM	[36]
SNC-900	100–5000 μM	80 μM	[37]
CuCo_2O_4	1–10 μM	0.573 μM	[38]
TPyP-CuS	1–30 μM	0.419 μM	[39]
CuO NPs-POM	0.02–500 μM	0.015 μM	[40]
Zn/Mo DSAC-SMA	0.1–5000 μM	0.76 μM	[41]
Au/T15/Pt	1.25–22.5 μM	0.853 μM	[42]

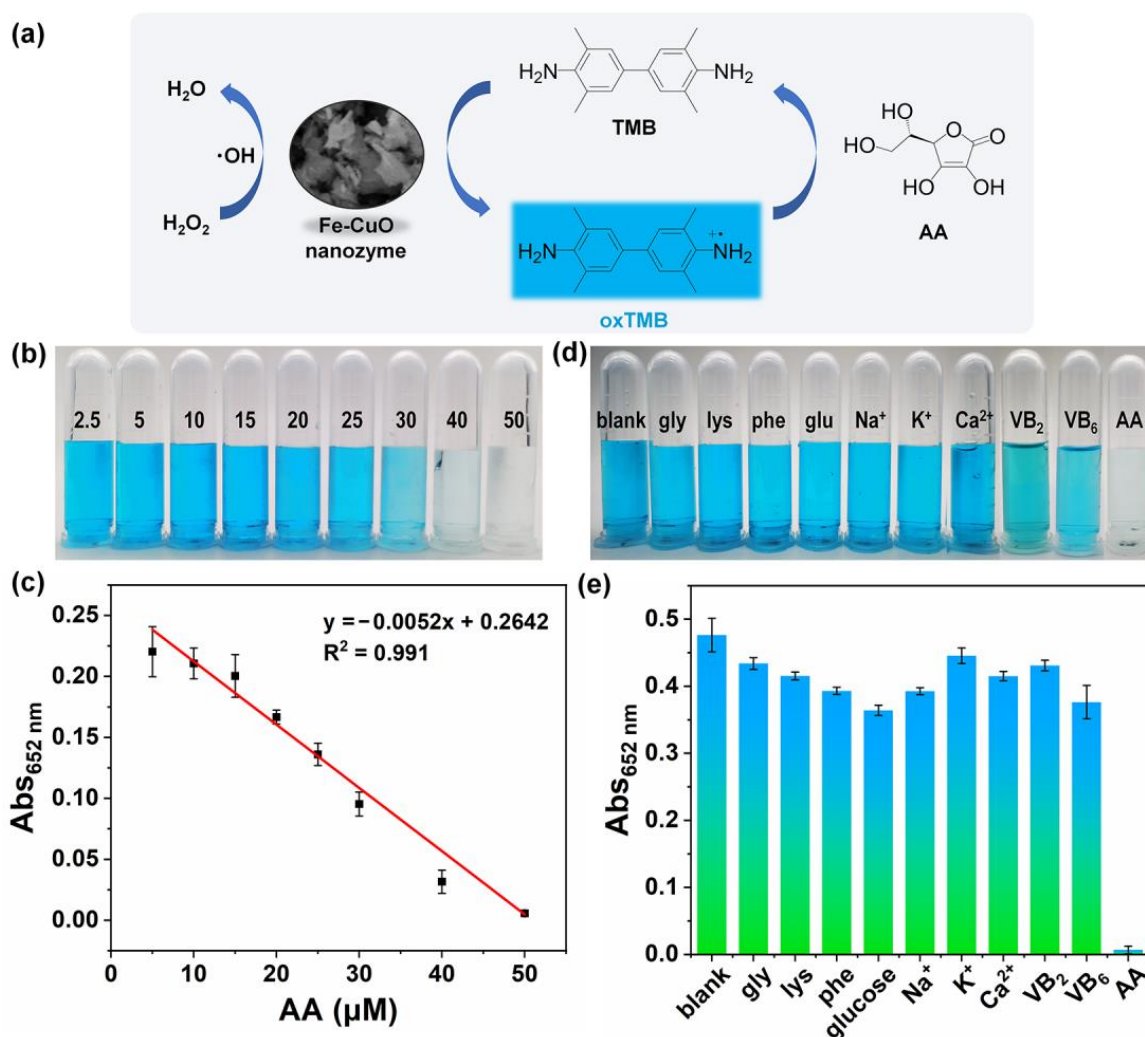


Figure 9. (a) Schematic illustration of the colorimetric detection of AA based on the POD-like activity of Fe-CuO nanozymes. (b) Digital photograph of the resultant systems in the presence of AA with different concentrations (2.5, 5, 10, 15, 20, 25, 30, 40, and 50 μM). (c) Linear calibration plot for AA detection from 5 to 50 μM . For sensitivity evaluation, the reactions of 3 mL system containing 120 $\mu\text{g}\cdot\text{mL}^{-1}$ TMB, 150 μM H_2O_2 , and 90 $\mu\text{g}\cdot\text{mL}^{-1}$ Fe-CuO nanozyme in 0.2 M acetate buffer (pH 4.0) were conducted at 25 $^\circ\text{C}$ for 5 min. (d) Digital photograph of the resultant systems in the presence of gly, lys, phe, glucose, Na^+ , K^+ , Ca^{2+} , vitamin B6, vitamin B2, and AA. (e) Selectivity of the TiO_2 PNZ-based colorimetric sensor for the determination of AA. For selectivity evaluation, the reactions of 3 mL system containing 120 $\mu\text{g}\cdot\text{mL}^{-1}$ TMB, 5 mM H_2O_2 , 90 $\mu\text{g}\cdot\text{mL}^{-1}$ Fe-CuO nanozyme, and 500 μM AA or 1000 μM interferences in 0.2 M acetate buffer (pH 4.0) were conducted at 25 $^\circ\text{C}$ for 5 min. Error bars in panel (c,d) are the standard deviations of three parallel experiments.

To validate the selectivity of the proposed colorimetric AA sensing system, a variety of possible interferences, including amino acids, glucose, metal ions, and other vitamin molecules, were challenged (Figure 9d). As expected, only the presence of AA results in a significant decrease in the absorbance at the same substrate concentration (Figure 9e). This selectivity test substantiates that the proposed detection strategy has excellent specificity for AA. Therefore, the above results indicate that highly sensitive and selective AA detection with Fe-CuO nanozymes has a good usability.

3.7. Practicability for TAC Assay in Real-World Scenarios

As a critical indicator for estimating antioxidants in antioxidant foods and medicines, the sensitive determination of TAC is attractive [36,37]. AA is usually selected to be the antioxidative model for a TAC assay. With the sensing strategy proposed in this work, we developed a TAC biosensor for real-world samples to verify the feasibility of the Fe-CuO nanozyme-based biosensor for practical usage [43]. For example, Mizone is one of the popular functional sports drinks produced by Danone. After appropriate dilution of the commercial beverage, the content of equivalent AA was detected using the proposed method, followed by the spiked recovery experiments using the standard addition method to verify the accuracy of our biosensor (Table 3). It is found that the concentration of equivalent AA in Mizone is 59.1 mM. Moreover, the recoveries of the standard AA are in the range of 98% to 104%, while the corresponding relative standard deviations (RSD) of three repetitive experiments are less than 10%. Thus, the competency of the Fe-CuO nanozyme-based biosensor for TAC assays in practical applications is proved.

Table 3. Quantification of equivalent AA in the real-world sample with Fe-CuO nanozymes.

Sample	Detected (μM) *	Added (μM)	Found (μM)	Recovery (%)	RSD (%)
Mizone	14.78 \pm 0.58	10.00	9.872 \pm 0.916	98.70	9.3
		15.00	15.26 \pm 0.35	101.7	2.3
		20.00	20.77 \pm 1.24	103.8	6.0

* The commercial drink was diluted 40 times for detection.

4. Conclusions

In summary, we developed a facile strategy to synthesize Fe-CuO nanozymes, in which the doping of Fe can enhance the POD-like activity of CuO. Working as an effective nanocatalyst, Fe-CuO can promote the chromogenic oxidation reaction between TMB and H₂O₂. Based on the splendid POD-like activity, a proof-of-concept colorimetric sensing platform for AA detection was established. The proposed sensing strategy exhibits a LOD of 4.66 μM and excellent anti-interference ability. The current work provides a facile metal-doping method to prepare effective CuO-based nanozymes with improved catalytic activity, which also extends the toolkit for building facile biosensors.

Author Contributions: Conceptualization, J.L. and K.L.; Methodology, B.Y. and J.L.; Validation, J.L.; Formal Analysis, B.Y., Y.Y. and Y.X.; Investigation, B.Y., Y.Y. and Y.X.; Data Curation, B.Y., Y.Y. and Y.X.; Writing—Original Draft Preparation, B.Y. and K.L.; Writing—Review and Editing, K.L.; Visualization, B.Y. and Y.Y.; Supervision, K.L.; Project Administration, J.L. and K.L.; Funding Acquisition, K.L. All authors have read and agreed to the published version of the manuscript.

Funding: This research was funded by the National Natural Science Foundation of China (No. 22074038) and the Fundamental Research Funds for the Central Universities.

Data Availability Statement: Data are available upon reasonable request from the authors.

Acknowledgments: Yan Zhang, Wenlong Tan, Xuyan Yao, Jinsong Fan, and Pingping Wan are acknowledged for operating the instruments for characterization.

Conflicts of Interest: The authors declare no conflict of interest.

References

- Geng, C.; Huang, Y.; Li, B.; Wang, Y.; Zhu, L.; Xu, Y.; Gao, K.; Mu, Y.; Su, Y.; Deng, S.; et al. Point-of-Care Testing of Chloramphenicol in Food Production Using Smartphone-Based Electrochemical Detector. *J. Anal. Test.* **2022**, *7*, 33–39. [[CrossRef](#)]
- Xiao, X.; Wu, K.; Yan, A.; Wang, J.G.; Zhang, Z.; Li, D. Intelligent Probabilistic System for Digital Tracing Cellular Origin of Individual Clinical Extracellular Vesicles. *Anal. Chem.* **2021**, *93*, 10343–10350. [[CrossRef](#)] [[PubMed](#)]
- Peng, X.-X.; Qin, X.; Qin, Y.; Xiang, Y.; Zhang, G.-J.; Yang, F. Bioprobes-regulated precision biosensing of exosomes: From the nanovesicle surface to the inside. *Coord. Chem. Rev.* **2022**, *463*, 214538. [[CrossRef](#)]
- Liang, T.-T.; Qin, X.; Xiang, Y.; Tang, Y.; Yang, F. Advances in nucleic acids-scaffolded electrical sensing of extracellular vesicle biomarkers. *TrAC Trends Anal. Chem.* **2022**, *148*, 116532. [[CrossRef](#)]

5. Wu, H.; Zhang, C.; Zhu, F.; Zhu, Y.; Lu, X.; Wan, Y.; Su, S.; Chao, J.; Wang, L.; Zhu, D. Programmably engineered FRET-nanoflare for ratiometric live-cell ATP imaging with anti-interference capability. *Chem. Commun.* **2023**, *59*, 4047–4050. [[CrossRef](#)]
6. Wang, C.; Yan, A.; Wang, H.; Su, Y.; Li, D. DNA-Mediated Membrane Fusion and Its Biological Applications: Sensing, Reaction Control and Drug Delivery. *Anal. Sens.* **2022**, *2*, e202200024. [[CrossRef](#)]
7. Pan, H.; Dong, Y.; Gong, L.; Zhai, J.; Song, C.; Ge, Z.; Su, Y.; Zhu, D.; Chao, J.; Su, S.; et al. Sensing gastric cancer exosomes with MoS₂-based SERS aptasensor. *Biosens. Bioelectron.* **2022**, *215*, 114553. [[CrossRef](#)]
8. Wang, Y.; Wang, S.; Dong, N.; Kang, W.; Li, K.; Nie, Z. Titanium Carbide MXenes Mediated In Situ Reduction Allows Label-Free and Visualized Nanoplasmonic Sensing of Silver Ions. *Anal. Chem.* **2020**, *92*, 4623–4629. [[CrossRef](#)]
9. Gao, L.; Zhuang, J.; Nie, L.; Zhang, J.; Zhang, Y.; Gu, N.; Wang, T.; Feng, J.; Yang, D.; Perrett, S.; et al. Intrinsic peroxidase-like activity of ferromagnetic nanoparticles. *Nat. Nanotechnol.* **2007**, *2*, 577–583. [[CrossRef](#)]
10. Wang, H.W.a.E. Fe₃O₄ Magnetic Nanoparticles as Peroxidase Mimetics and Their Applications in H₂O₂ and Glucose Detection. *Anal. Chem.* **2008**, *80*, 2250–2254. [[CrossRef](#)]
11. Zhou, Y.; Liu, C.; Yu, Y.; Yin, M.; Sun, J.; Huang, J.; Chen, N.; Wang, H.; Fan, C.; Song, H. An Organelle-Specific Nanozyme for Diabetes Care in Genetically or Diet-Induced Models. *Adv. Mater.* **2020**, *32*, e2003708. [[CrossRef](#)] [[PubMed](#)]
12. Du, Y.; Ke, Z.; Zhang, J.; Feng, G. Dual-signal output paper sensor based on coordinative self-assembly biomimetic nanozyme for point-of-care detection of biomarker. *Biosens. Bioelectron.* **2022**, *216*, 114656. [[CrossRef](#)] [[PubMed](#)]
13. Zandieh, M.; Liu, J. Removal and Degradation of Microplastics Using the Magnetic and Nanozyme Activities of Bare Iron Oxide Nanoaggregates. *Angew. Chem. Int. Ed.* **2022**, *61*, e202212013. [[CrossRef](#)] [[PubMed](#)]
14. Lin, S.; Tan, W.; Han, P.; Li, X.; Li, J.; Nie, Z.; Li, K. A photonanozyme with light-empowered specific peroxidase-mimicking activity. *Nano Res.* **2022**, *15*, 9073–9081. [[CrossRef](#)]
15. Li, X.; Zhang, Y.; Tan, W.; Jin, P.; Zhang, P.; Li, K. Bioinspired Coassembly of Copper Ions and Nicotinamide Adenine Dinucleotides for Single-Site Nanozyme with Dual Catalytic Functions. *Anal. Chem.* **2023**, *95*, 2865–2873. [[CrossRef](#)]
16. Wu, J.; Wei, H. Efficient Design Strategies for Nanozymes. *Prog. Chem.* **2020**, *33*, 42–51. [[CrossRef](#)]
17. Zandieh, M.; Liu, J. Surface Science of Nanozymes and Defining a Nanozyme Unit. *Langmuir* **2022**, *38*, 3617–3622. [[CrossRef](#)]
18. Zandieh, M.; Liu, J. Nanozymes: Definition, Activity, and Mechanisms. *Adv. Mater.* **2023**, e2211041. [[CrossRef](#)]
19. Jiang, D.; Ni, D.; Rosenkrans, Z.T.; Huang, P.; Yan, X.; Cai, W. Nanozyme: New horizons for responsive biomedical applications. *Chem. Soc. Rev.* **2019**, *48*, 3683–3704. [[CrossRef](#)]
20. Wu, J.; Wang, X.; Wang, Q.; Lou, Z.; Li, S.; Zhu, Y.; Qin, L.; Wei, H. Nanomaterials with enzyme-like characteristics (nanozymes): Next-generation artificial enzymes (II). *Chem. Soc. Rev.* **2019**, *48*, 1004–1076. [[CrossRef](#)]
21. Gao, M.; Lu, X.; Chen, S.; Tian, D.; Zhu, Y.; Wang, C. Enhanced Peroxidase-like Activity of Mo⁶⁺-Doped Co₃O₄ Nanotubes for Ultrasensitive and Colorimetric L-Cysteine Detection. *ACS Appl. Nano Mater.* **2018**, *1*, 4703–4715. [[CrossRef](#)]
22. Chaudhary, M.; Singh, M.; Kumar, A.; Prachi; Gautam, Y.K.; Malik, A.K.; Kumar, Y.; Singh, B.P. Experimental investigation of Co and Fe-Doped CuO nanostructured electrode material for remarkable electrochemical performance. *Ceram. Int.* **2021**, *47*, 2094–2106. [[CrossRef](#)]
23. Zhang, X.; Yang, Q.; Lang, Y.; Jiang, X.; Wu, P. Rationale of 3,3',5,5'-Tetramethylbenzidine as the Chromogenic Substrate in Colorimetric Analysis. *Anal. Chem.* **2020**, *92*, 12400–12406. [[CrossRef](#)] [[PubMed](#)]
24. Wang, J.; Hu, Y.; Zhou, Q.; Hu, L.; Fu, W.; Wang, Y. Peroxidase-like Activity of Metal-Organic Framework [Cu(PDA)(DMF)] and Its Application for Colorimetric Detection of Dopamine. *ACS Appl. Mater. Interfaces* **2019**, *11*, 44466–44473. [[CrossRef](#)]
25. Zhang, R.; Lu, N.; Zhang, J.; Yan, R.; Li, J.; Wang, L.; Wang, N.; Lv, M.; Zhang, M. Ultrasensitive aptamer-based protein assays based on one-dimensional core-shell nanozymes. *Biosens Bioelectron.* **2020**, *150*, 111881. [[CrossRef](#)]
26. Peng, H.; Zhang, J.; Zeng, C.; Zhou, C.; Li, Q.; Lu, N.; Wang, L. One-Dimensional Synergistic Core-Shell Nanozymes with Superior Peroxidase-like Activity for Ultrasensitive Colorimetric Detection of Blood Cholesterol. *ACS Appl. Bio Mater.* **2020**, *3*, 5111–5119. [[CrossRef](#)]
27. He, Y.; Li, N.; Liu, X.; Chen, W.; Zhu, X.; Liu, Q. 5,10,15,20-tetrakis (4-carboxyl phenyl) porphyrin-functionalized urchin-like CuCo₂O₄ as an excellent artificial nanozyme for determination of dopamine. *Microchim. Acta* **2021**, *188*, 171. [[CrossRef](#)]
28. Jiao, A.; Xu, L.; Tian, Y.; Cui, Q.; Liu, X.; Chen, M. Cu₂O nanocubes-grafted highly dense Au nanoparticles with modulated electronic structures for improving peroxidase catalytic performances. *Talanta* **2021**, *225*, 121990. [[CrossRef](#)]
29. Zhu, Z.; Gong, L.; Miao, X.; Chen, C.; Su, S. Prussian Blue Nanoparticle Supported MoS₂ Nanocomposites as a Peroxidase-Like Nanozyme for Colorimetric Sensing of Dopamine. *Biosensors* **2022**, *12*, 260. [[CrossRef](#)]
30. Wang, M.; Zhao, Z.; Gong, W.; Zhang, M.; Lu, N. Modulating the Biomimetic and Fluorescence Quenching Activities of Metal-Organic Framework/Platinum Nanoparticle Composites and Their Applications in Molecular Biosensing. *ACS Appl. Mater. Interfaces* **2022**, *14*, 21677–21686. [[CrossRef](#)]
31. Hao, P.; Liu, Y.; Wang, L.; Zhu, X.; Liu, Q. Nanozyme Sensor Array Based on Porphyrin-Modified CoMoO₄ to Detect and Distinguish Biologically Important Thiols. *ACS Appl. Nano Mater.* **2023**, *6*, 1937–1947. [[CrossRef](#)]
32. Hao, P.; Liu, Y.; Dong, S.; Fan, G.; Li, G.; Xie, M.; Liu, Q. Enhanced peroxidase-like activity of 2(3), 9(10), 16(17), 23(24)-octamethoxyphthalocyanine modified CoFe LDH for a sensor array for reducing substances with catechol structure. *Anal. Bioanal. Chem.* **2023**, *415*, 289–301. [[CrossRef](#)] [[PubMed](#)]
33. Liu, H.; Ding, Y.-N.; Yang, B.; Liu, Z.; Zhang, X.; Liu, Q. Iron Doped CuSn(OH)₆ Microspheres as a Peroxidase-Mimicking Artificial Enzyme for H₂O₂ Colorimetric Detection. *ACS Sustain. Chem. Eng.* **2018**, *6*, 14383–14393. [[CrossRef](#)]

34. Qileng, A.; Zhu, H.; Liu, S.; He, L.; Qin, W.; Liu, W.; Xu, Z.; Liu, Y. Machine learning: Assisted multivariate detection and visual image matching to build broad-specificity immunosensor. *Sens. Actuators B Chem.* **2021**, *339*, 129872. [[CrossRef](#)]
35. Chen, H.; Cai, Z.; Gui, J.; Tang, Y.; Yin, P.; Zhu, X.; Zhang, Y.; Li, H.; Liu, M.; Yao, S. A redox reaction-induced ratiometric fluorescence platform for the specific detection of ascorbic acid based on Ag₂S quantum dots and multifunctional CoOOH nanoflakes. *J. Mater. Chem. B* **2023**, *11*, 1279–1287. [[CrossRef](#)] [[PubMed](#)]
36. Lou, Z.; Zhao, S.; Wang, Q.; Wei, H. N-Doped Carbon As Peroxidase-Like Nanozymes for Total Antioxidant Capacity Assay. *Anal. Chem.* **2019**, *91*, 15267–15274. [[CrossRef](#)]
37. Chen, Y.; Jiao, L.; Yan, H.; Xu, W.; Wu, Y.; Wang, H.; Gu, W.; Zhu, C. Hierarchically Porous S/N Codoped Carbon Nanozymes with Enhanced Peroxidase-like Activity for Total Antioxidant Capacity Biosensing. *Anal. Chem.* **2020**, *92*, 13518–13524. [[CrossRef](#)]
38. Han, S.; Chen, X.; Fan, Y.; Zhang, Y.; Yang, Z.; Kong, X.; Liu, Z.; Liu, Q.; Zhang, X. The excellent peroxidase-like activity of uniform CuCo₂O₄ microspheres with oxygen vacancy for fast sensing of hydrogen peroxide and ascorbic acid. *New J. Chem.* **2021**, *45*, 2030–2037. [[CrossRef](#)]
39. He, Y.; Li, N.; Lian, J.; Yang, Z.; Liu, Z.; Liu, Q.; Zhang, X.; Zhang, X. Colorimetric ascorbic acid sensing from a synergetic catalytic strategy based on 5,10,15,20-tetra(4-pyridyl)-21H,23H-porphyrin functionalized CuS nanohexahedrons with the enhanced peroxidase-like activity. *Colloids Surfaces A Physicochem. Eng. Asp.* **2020**, *598*, 124855. [[CrossRef](#)]
40. Xu, Y.; Li, P.; Hu, X.; Chen, H.; Tang, Y.; Zhu, Y.; Zhu, X.; Zhang, Y.; Liu, M.; Yao, S. Polyoxometalate Nanostructures Decorated with CuO Nanoparticles for Sensing Ascorbic Acid and Fe²⁺ Ions. *ACS Appl. Nano Mater.* **2021**, *4*, 8302–8313. [[CrossRef](#)]
41. Ma, C.B.; Xu, Y.; Wu, L.; Wang, Q.; Zheng, J.J.; Ren, G.; Wang, X.; Gao, X.; Zhou, M.; Wang, M.; et al. Guided Synthesis of a Mo/Zn Dual Single-Atom Nanozyme with Synergistic Effect and Peroxidase-like Activity. *Angew. Chem. Int. Ed.* **2022**, *61*, e202116170. [[CrossRef](#)] [[PubMed](#)]
42. Cai, M.; Zhang, Y.; Cao, Z.; Lin, W.; Lu, N. DNA-Programmed Tuning of the Growth and Enzyme-Like Activity of a Bimetallic Nanozyme and Its Biosensing Applications. *ACS Appl. Mater. Interfaces* **2023**, *15*, 18620–18629. [[CrossRef](#)] [[PubMed](#)]
43. Gooding, J. What Is a “Real Sample”? *ACS Sens.* **2018**, *3*, 1609. [[CrossRef](#)] [[PubMed](#)]

Disclaimer/Publisher’s Note: The statements, opinions and data contained in all publications are solely those of the individual author(s) and contributor(s) and not of MDPI and/or the editor(s). MDPI and/or the editor(s) disclaim responsibility for any injury to people or property resulting from any ideas, methods, instructions or products referred to in the content.